Since January 2020 Elsevier has created a COVID-19 resource centre with free information in English and Mandarin on the novel coronavirus COVID-19. The COVID-19 resource centre is hosted on Elsevier Connect, the company's public news and information website.

Journal of Molecular Structure 1250 (2022) 131853

Contents lists available at ScienceDirect

Journal of Molecular Structure

journal homepage: www.elsevier.com/locate/molstr

New thiophene-derived α-aminophosphonic acids: Synthesis under microwave irradiations, antioxidant and antifungal activities, DFT investigations and SARS-CoV-2 main protease inhibition

Hamida Tlidjane[a], Nadjib Chafai[a,*], Salah Chafaa[a], Chawki Bensouici[b], Khalissa Benbouguerra[a]

[a] Laboratory of Electrochemistry of Molecular Materials and Complex (LEMMC). Department of Process Engineering, Faculty of Technology, University of Ferhat ABBAS Setif-1, El-Mabouda campus, 19000 Sétif, Algeria
[b] Centre de recherche en Biotecnologie, Ali Mendjli, Nouvelle Ville UV 03, BP E73 Constantine, Algeria

ARTICLE INFO

Article history:
Received 22 September 2021
Revised 28 October 2021
Accepted 30 October 2021
Available online 3 November 2021

Keywords:
α-Aminophosphonates
Antioxidant
Anti-fungal
DFT
Molecular docking
COVID-19

ABSTRACT

Four new α-aminophosphonic acids containing thiophene ring have been synthesized using simple, neat and catalyst-free conditions, more convenient and eco-friendly method under microwave irradiations. The structures of the title molecules have been confirmed by UV-Vis, FT-IR, ^{1}H NMR, ^{13}C NMR and ^{31}P NMR. Moreover, their antioxidant activity was evaluated using DPPH, ABTS and phenantroline methods; the obtained results indicate that the title molecules exhibit excellent activity better than standards BHT and BHA. Also, the synthesized compounds show a good antifungal activity against two fungi, *Fusarium oxysporum* and *Alternaria alternata*. In addition, molecular, electronic properties, stability and reactivity of the synthesized products were studied by the density functional theory (DFT). Furthermore, molecular docking investigations of the studied α-aminophosphonic acids showed a good inhibition of SARS-CoV-2 main protease (Mpro).

1. Introduction

In late December 2019, a novel Coronavirus disease (COVID-19) caused by SARS-CoV-2 virus was identified in Wuhan, China [1]. This virus is crown-shaped and has a diameter of 60-140 nm [2]. COVID-19 spread rapidly, becoming deadly in several countries [3] which confused the whole world and it becomes an epidemic [4]. Two months later, it turned into a pandemic.

The search for vaccines and drugs continues, which led us to synthesis new bioactive molecules called α-aminophosphonates, structural analogues of the corresponding α-amino-acids [5]. Generally, α-aminophosphonates have a wide applications in ~~the~~ different fields such as medicinal chemistry, industry and agriculture which may act as antiviral [6, 7], cytotoxic to cancer cells [8–10], enzyme inhibitors [11], herbicide [12] and fungicide [13]. In addition, the aromatic α-aminophosphonates containing thiophene heterocyclic rings are also very attractive and exhibit important biological activities [14–16].

As a result, many methods for the preparation of diverse α-aminophosphonates have been published using catalysts such as $FeCl_3$ [17–19], $CoCl_2$ [20], $TaCl_5$-SiO_2 [21], $InCl_3$ [22] and TiO_2 [23]. Furthermore, the ultrasound irradiation and microwave are considered as a successful alternative protocol to synthesis α-aminophosphonates in good yields [24–27]. As part of our series of research in our laboratory [28–30], we recently reported investigations on the course of microwave irradiations applied in organic synthesis which has several advantages such as easy workup, reducing the reaction time from days to minutes, cleaner products, higher yields and environmentally benign which attract and encourage the organic chemists to use this method [31–33].

The biological and chemical activities of α-aminophosphonates can be affected by their electronic and physicochemical characteristics. In this context, the Density Functional Theory (DFT) method is widely used to perform quantum chemical calculations and to establish the active sites of organic compounds [34–36]. Also, the molecular docking plays an important role in the design of new drugs [37].

In the present work, we report the synthesis of a new series of α-aminophosphonic acids. Also, their molecular structures have been determined using spectroscopic methods such as UV-Vis, FT-IR, ^{1}H NMR, ^{13}C NMR, and ^{31}P NMR. The antioxidant activity of the synthesized α-aminophosphonic acids has been evaluated by DPPH, ABTS and phenantroline methods. In addition,

* Corresponding author.
E-mail addresses: n.chafai@univ-setif.dz, nadjib82@gmail.com (N. Chafai).

https://doi.org/10.1016/j.molstruc.2021.131853
0022-2860/

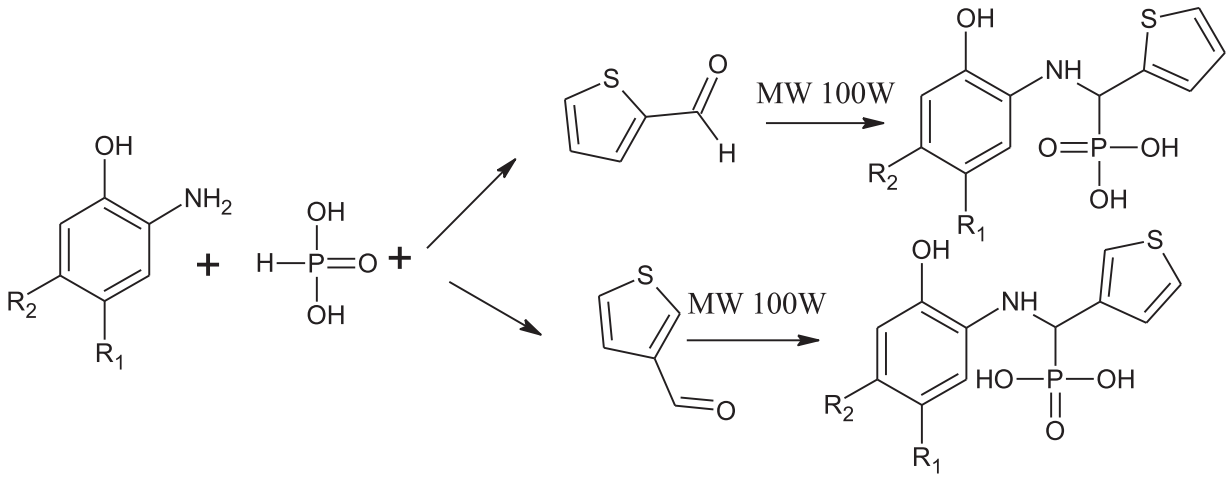

Fig. 1. Synthesis sequences of α-aminophosphonic acids with (5N2TPA, 5N3TPA: R_1=H, R_2=NO_2, 4M3TPA: R_1= CH_3, R_2= H, 5M3TPA: R_1=H, R_2= CH_3)

the antifungal activity against two fungi such as *Fusarium oxysporum* and *Alternaria alternate* was determined. Moreover, the optimized geometries, frontiers molecular orbitals, Mulliken charges have been constructed to understand the electronic properties of the title molecules using DFT calculations. In addition, the synthesized α-aminophosphonic acids were screened theoretically to explore binding affinity, binding modes and molecular interactions against SARS-CoV-2 main protease (Mpro) using molecular docking.

2. Experimental

2.1. Chemicals/instrumentations

All chemicals were purchased from Sigma-Aldrich and used without purification. All reactions were monitored by thin-layer chromatography (TLC) on silica Merck GF254 plates. Microwave assisted reactions were carried out using MWO720CR6S microwave. The melting points (m. p) of the obtained α-aminophosphonic acids were measured by open capillary method in BÜCHI melting point B-540. UV-Vis spectra in ethanol were measured with a UV-Vis spectrophotometer (V-650 Jasco double beam). The FT-IR spectra were recorded in transmittance mode from 4000 to 600 cm^{-1} on a spectrometer type: FT-IR-4200 Jasco. ^{1}H NMR, ^{13}C NMR and ^{31}P NMR are recorded on a Bruker spectrometer at 400, 133, 100 MHz, respectively using DMSO-d_6 as solvent. Chemical shifts are reported in units (ppm) with tetramethylsilane (TMS) as a reference.

2.2. General procedure for the synthesis of α-aminophosphonic acids

In this paper, new categories of α-aminophosphonic acids were synthesized using four substituted aminophenols (nitro and methyl group with two position *orto* and *para*), two aldehydes (2-thiophenecarboxaldehyde and 3-thiophenecarboxaldehyde) and phosphorous acid. Briefly, a mixture of 1 mmol of amine was dissolved in ethanol and treated with phosphorous acid (1 mmol), then thiophene carboxaldehyde (1 mmol) was added drop wise, and the mixture was irradiated in microwave (100 watts) for 3-8 min (Fig. 1). Completion of the reaction was monitored by TLC analysis. Finally, the crude product was purified in ethanol and cooled at room temperature. The synthesized α-aminophosphonic acids are obtained in good yields (Table 1) and their structures were determined using UV-Vis, FT-IR, ^{1}H NMR, ^{13}C NMR and ^{31}P NMR spectra.

2.3. Analytical data

2.3.1. {[(2-hydroxy-4-nitrophenyl) amino] (thiophen-2-yl) methyl} phosphonic acid (5N2TPA)

Black crystalline powder; Yield: 96.96 %; m.p 159.6°C; **UV-Vis** (EtOH), $\lambda_{max\ (n)}$ (nm): $\lambda_{max(1)}$ (392.84), $\lambda_{max(2)}$ (264.05), $\lambda_{max(3)}$ (217.44); **IR** (solid state), ν(cm^{-1}): 3597 (O-H), 3376 (N-H), 1610 (C=C $_{aromatic}$), 1252 (P=O), 1015 (C-N), 930 (P-O-H), 749 (P-C); **^{1}H NMR** (400 MHz, DMSO-d_6), δ (ppm): 1.24 (1H, d, N-C **H**), 5.93 (2H, s, P-O- **H**), 6.60 (1H, s, -C **H**$_{Ar}$-), 6.63 (1H, s, -C **H**$_{Ar}$-), 7.49 (1H, d, -C **H**$_{Ar}$-), 7.53 (1H, s, -C **H**$_{Ar}$-), 7.59 (1H, d, -C **H**$_{Ar}$-), 7.61 (1H, d, -C **H**$_{Ar}$-), 9.50 (1H, s, N- **H**), 9.91(1H, s, -O **H**); **^{13}C NMR** (133 MHz, DMSO-d_6), δ (ppm): 109.14 (2C, - **C**H$_{Ar}$), 111.64 (2C, - **C**H$_{Ar}$), 118.76 (2C, - **C**H$_{Ar}$), 136.03 (1C, - **C**H$_{Ar}$), 142.92 (2C, - **C**H$_{Ar}$), 146.01 (2C, - **C**H$_{Ar}$); **^{31}P NMR** δ (ppm): 3.10.

2.3.2. {[(2-hydroxy-4-nitrophenyl) amino] (thiophen-3-yl) methyl} phosphonic acid (5N3TPA)

Brown Crystals; Yield 95.75 %; m.p 148.8°C; **UV-Vis** (EtOH), $\lambda_{max\ (n)}$ (nm): $\lambda_{max(1)}$ (392.84), $\lambda_{max(2)}$ (264.05), $\lambda_{max(3)}$ (217.44); **IR** (solid state), ν (cm^{-1}): 3594 (O-H), 3383 (N-H), 1606 (C=C $_{aromatic}$), 1276 (P=O), 1002 (C-N), 930 (P-O-H), 742 (P-C); **^{1}H NMR** (400 MHz, DMSO-d_6), δ (ppm): 1.24 (1H, d, N-C **H**), 5.92 (2H, s, P-O- **H**), 6.60 (1H, s, -C **H**$_{Ar}$-), 6.62 (1H, s, -C **H**$_{Ar}$-), 7.48 (1H, s, -C **H**$_{Ar}$-), 7.53 (1H, s, -C **H**$_{Ar}$-), 7.58 (1H, s, -C **H**$_{Ar}$-), 7.60 (1H, s, -C **H**$_{Ar}$-), 9.50 (1H, s, N- **H**), 10.01 (1H, s, -O **H**); **^{13}C NMR** (133 MHz, DMSO-d_6), δ (ppm): 109.14 (2C,- **C**H$_{Ar}$), 111.65 (2C, - **C**H$_{Ar}$), 118.76 (2C, - **C**H$_{Ar}$), 136.03 (2C, - **C**H$_{Ar}$), 142.91 (2C, - **C**H$_{Ar}$), 146.01 (2C, - **C**H$_{Ar}$); **^{31}PNMR** δ (ppm): 3.51.

2.3.3. {[(2-hydroxy-5-methylphenyl) amino] (thiophen-3-yl) methyl} phosphonic acid (4M3TPA)

Yellow Crystalline powder; Yield 86.95 %; m.p 188°C; **UV-Vis** (EtOH), $\lambda_{max\ (n)}$ (nm): $\lambda_{max(1)}$ (278.54), $\lambda_{max(2)}$ (225.13), $\lambda_{max(3)}$ (209.57); **IR** (solid state),ν (cm^{-1}): 3577 (O-H), 3321 (N-H), 1605 (C=C $_{aromatic}$), 1262 (P=O), 1000 (C-N), 930 (P-O-H), 720 (P-C); **^{1}H NMR** (400 MHz, DMSO-d_6), δ (ppm): 2.08 (3H, s, C **H** **3**-), 1.23 (1H, s, C **H**-), 4.25 (1H, s, N **H**-), 5.91 (2H, s, P-O- **H**), 6.23 (1H, d, -C **H**$_{Ar}$-), 6.25 (1H, d, -C **H**$_{Ar}$-), 6.43 (1H, d, -C **H**$_{Ar}$-), 6.51(1H, s, -C **H**$_{Ar}$-), 6.53 (1H, s, -C **H**$_{Ar}$-), 7.5 (1H, s, N- **H**-), 8.7 (1H, s, -O **H**); **^{13}C NMR** (133 MHz, DMSO-d_6), δ (ppm): 20.75 (1C, **C**H$_3$), 114.86 (3C, - **C**H$_{Ar}$), 116.33 (2C, - **C**H$_{Ar}$), 118.11 (1C, - **C**H$_{Ar}$), 128.31 (2C, - **C**H$_{Ar}$), 135.46 (1C, - **C**H$_{Ar}$), 142 (2C, - **C**H$_{Ar}$); **^{31}PNMR** δ (ppm): 3.19.

Table 1
Yields and synthesis time of the studied α-aminophosphonic acids under microwave irradiations.

Molecule	R_1	R_2	Aldehyde	Molecular weight (g/mol)	Time (min)	Yield (%)
5N2TPA	H	NO_2	2-thiophene- carboxaldehyde	330	8 min	96.96
5N3TPA	H	NO_2	3-thiophene- carboxaldehyde	330	4 min	95.75
4M3TPA	CH_3	H	3-thiophene- carboxaldehyde	299	0 min	86.95
5M3TPA	H	CH_3	3-thiophene- carboxaldehyde	299	3 min 30s	96.98

Table 2
Experimental values of wavenumber and their assignments for the selected vibrations of 5N2TPA, 5N3TPA, 4M3TPA and 5M3TPA.

5N2TPA		5N3TPA		4M3TPA		5M3TPA	
Assignment	Vibrational frequency (cm^{-1})	Assignment	Vibrational frequency (cm^{-1})	Assignment	Vibrational frequency (cm^{-1})	Assignment	Vibrational frequency (cm^{-1})
ν O−H	3597	ν O−H	3594	ν O−H	3577	ν O−H	3586
ν N−H	3376	ν N−H	3383	ν N−H	3321	ν N−H	3337
ν C−H_{Ar}	3096	ν C−H_{Ar}	3093	ν C−H_{Ar}	3011	ν C−H_{Ar}	3062
ν_s C−H_{Alph}	2916	ν_s C−H_{Alph}	2902	ν_s C−H_{Alph}	2901	ν_s C−H_{Alph}	2924
ν_{as} C−H_{Alph}	2918	ν_{as} C−H_{Alph}	2982	ν_{as} C−H_{Alph}	2985	ν_{as} C−H_{Alph}	2886
ν P−OH	930	ν P−OH	928	ν P−OH	945	ν P−OH	943
ν N−C	1015	ν N−C	1002	ν N−C	1000	ν N−C	1002
ν P=O	1252	ν P=O	1276	ν P=O	1262	ν P=O	1276
ν C-P	749	ν C-P	742	ν C-P	720	ν C-P	742
ν C-C	1400	ν C-C	1399	ν C-C	1453	ν C-C	1428
ν C=C	1610	ν C=C	1606	ν C=C	1605	ν C=C	1615

ν: stretching, *s*: symmetric and *as*: asymmetric

Table 3
IC_{50} and $A_{0.5}$ values of the studied α-aminophosphonic acids and standards (BHT and BHA) determined by DPPH, $ABTS^+$ and Phenanthroline test.

Molecule	DPPH IC_{50} (µg/ml)	$ABTS^+$ IC_{50} (µg/ml)	Phenanthroline $A_{0.5}$ (µg/ml)
5N2TPA	26.15 ± 2.02	6.88 ± 2.13	25.16 ± 0.001
5N3TPA	16.04 ± 0.41	4.05 ± 1.13	5.57 ± 0.06
4M3TPA	21.12 ± 0.64	4.32 ± 2.78	10.36 ± 0.04
5M3TPA	22.06 ± 1.36	5.78 ± 1.38	16.54 ± 0.004
BHT	17.16 ± 2.01	1.27 ± 2.48	1.63 ± 0.06
BHA	6.60 ± 2.12	6.25 ± 0.5	7.20 ± 0.11

2.3.4. {[(2-hydroxy-4-methylphenyl) amino] (thiophen-3-yl) methyl} phosphonic acid (5M3TPA)

Black powder; Yield 96.98; m.p 180°C; **UV-Vis** (EtOH), $\lambda_{max\,(n)}$ (nm): $\lambda_{max(1)}$ (278.54), $\lambda_{max(2)}$ (225.13), $\lambda_{max(3)}$ (209.57); **IR** (solid state), ν (cm^{-1}): 3586 (O-H), 3337 (N-H), 1615 (C=C $_{aromatic}$), 1276 (P=O), 1002 (C-N), 930 (P-O-H), 742 (P-C); **^{1}H NMR** (400 MHz, DMSO-d_6): δ (ppm): 2.13 (3H, s, C **H** **3**-), 2.3 (1H, m, C **H**-), 5.91 (2H, s, P-O- **H**), 6.43 (1H, d, -C **H**$_{Ar}$-), 6.57 (1H, s, -C **H**$_{Ar}$-), 6.67 (1H, s, -C **H**$_{Ar}$-), 6.69 (1H, s, -C **H**$_{Ar}$-), 7.47 (1H, s, -C **H**$_{Ar}$-), 7.50 (1H, s, N- **H**), 7.6 (1H, s, -O **H**); **^{13}C NMR** (133 MHz, DMSO-d_6) δ (ppm): 20.75 (1C, **C**H_3), 116.01 (2C,- **C**H_{Ar}), 117.66 (2C, - **C**H_{Ar}), 120 (3C, - **C**H_{Ar}), 128.77 (1C, - **C**H_{Ar}), 129.93 (1C, - **C**H_{Ar}), 146.57 (2C, - **C**H_{Ar}); **^{31}PNMR** δ (ppm): 2.95.

2.4. Antioxidant activity

The antioxidant activity of the synthesized molecules was evaluated by three methods: DPPH, ABTS and phenantroline assay. The Methanol was used as negative control, while BHT (butylatedhydroxytoluene) and BHA (butylatedhydroxyanisole) were used as standards in the three methods. All tests were performed in 96-wells microplates using a Perkin Elmer, Enspire microplate reader and in triplicate.

2.4.1. Free radical scavenging activity (DPPH)

The radical scavenging activity of 5N2TPA, 5N3TPA, 4M3TPA and 5M3TPA was determined using the stable scavenger DPPH according to the method of Blois *et al* [38]. Briefly, a 40 µl of different concentrations (200, 100, 50, 25, 12.5, 6.25 and 3.125 µg/ml) of the studied molecules and standards prepared in methanol were added to 160 µl of methanol solution of DPPH (10^{-4} mol.L^{-1}) in triplicate. After that, the mixture was incubated in the dark for 30 min. The decrease in absorbance was measured against a blank (methanol) at 517 nm. The degree of DPPH-purple decolorization to DPPH-yellow indicated the scavenging efficiency of the tested samples. The percentage of inhibition of the various tested molecules was calculated using the following formula:

$$I\% = [(A\ blank - A\ sample)/A\ blank] \times 100$$

Where I% is the percentage of the antioxidant activity of the molecule, A_{blank} is the absorbance of the control (containing all reagents except the tested molecule), and A_{sample} is the absorbance of the sample. The 50 % inhibitory concentration value (IC_{50}) was calculated from the graph plotting inhibition percentage against sample concentration (Table 3).

2.4.2. ABTS essay

The radical scavenging activity against ABTS of the studied α-aminophosphonic acids was evaluated according to the method of Re *et al* [39]. The ABTS radical cation ($ABTS^{\bullet\,+}$) was produced by mixing ABTS (7 mM) and $K_2S_2O_8$ (2.45 mM) prepared in ethanol and the mixture was allow to stand for 12-16 hours in the dark at room temperature before use, the stock solution was diluted with ethanol to an absorbance of 0.700 ± 0.020 at 734 nm. 160 µl of ABTS working solution was mixed with 40 µl of different concentrations of the title molecules and standards (50, 25, 12.5, 6.25, 3.125, 1.5625 and 0.78125 µg/ml). The absorbance was measured after 10 min at 734 nm and the inhibition percentage was calculated using the same formula of the DPPH assay.

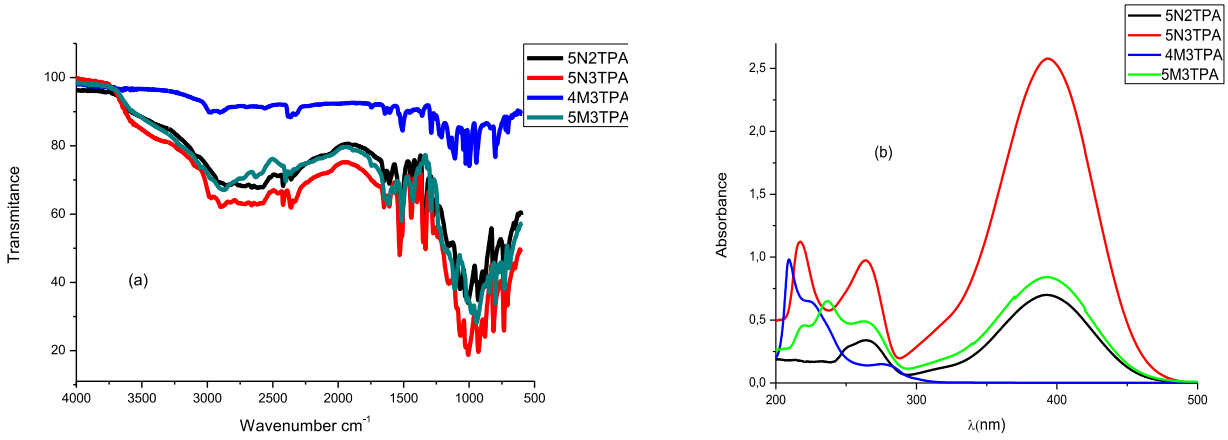

Fig. 2. Infrared (a) and UV-Vis (b) spectra of the synthesized molecules.

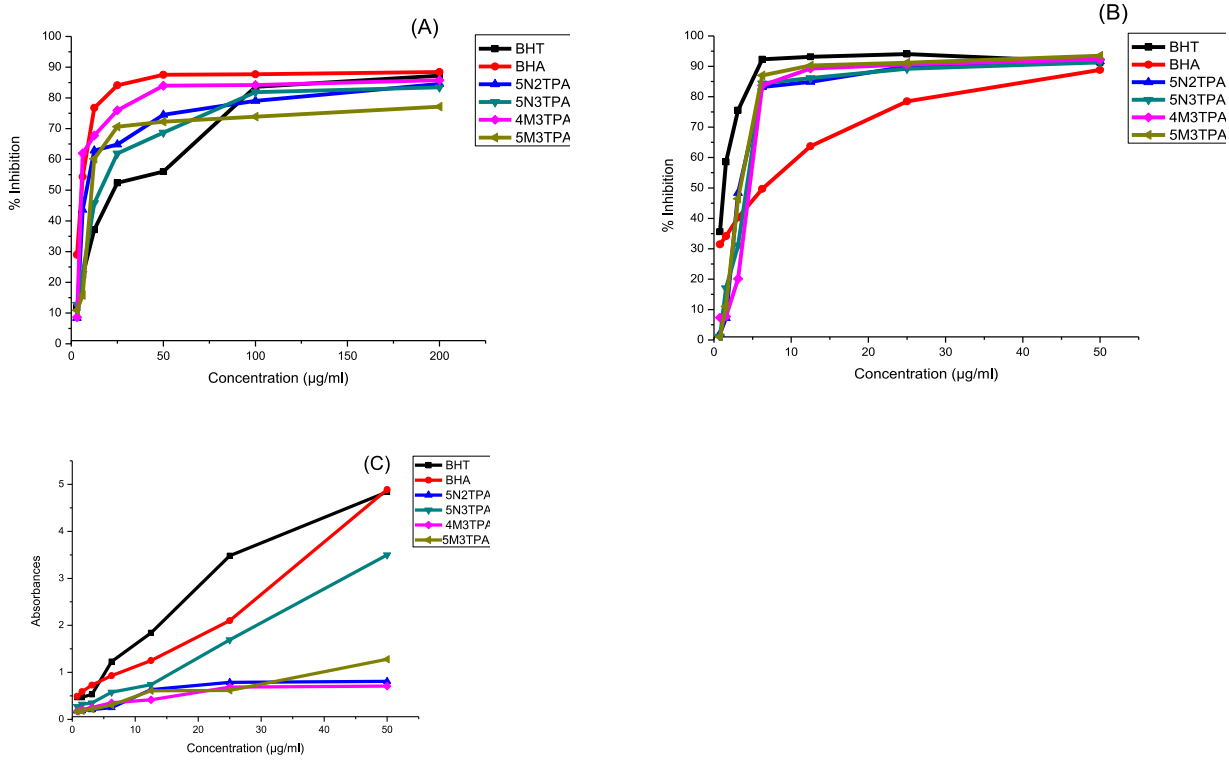

Fig. 3. The antioxidant activity of the studied molecules determined by three methods: DPPH (A), $ABTS^{+}$ (B) and Phenantroline (C).

2.4.3. Phenantroline essay

The antioxidant activity of the synthesized molecules was determined by the phenontroline test according to Szydlowska-Czerniaka *et al* [40]. Briefly, 50 µl of $FeCl_3$ (0.2%) was added to 30 µl of Phenanthroline (0.5%) then mixed with 110 µl of methanol and 10 µl of the different concentrations of samples and standards (50, 25, 12.5, 6.25, 3.125, 1.5625 and 0.78125 µg/ml). The mixture was incubated in the dark for 20 min at 30°C and the absorbance was measured at 510 nm. The results were given as absorbance (Fig. 3) and the 0.50 absorbance intensity ($A_{0.5}$) (Table 3).

2.5. Antifungal activity

The investigated α-aminophosphonic acids were screened for their antifungal activity against two pathogenic fungi: *Fusarium oxysporum* and *Alternaria alternata* by the disc diffusion method [41] in PDA (potato dextrose agar) medium at two concentrations (50 and 100 µg/ml) and in triplicate. A disc of 6 mm of diameter of the two pathogenic fungi was prepared and placed in the center of the Petri dishes which contain the PDA medium mixed with the samples at different concentrations and the Petri dishes were incubated at 25°C for 6 days. The molecules were diluted in DMSO for biological assays. DMSO was used as positive control and PDA only as negative control. The bioactivity was determined by measuring the diameter of the inhibition zone (DIZ) in mm and inhibition percentage (I%). Samples tested in triplicate and average results were recorded. The obtained results were presented in Tables 4 and 5 and compared with positive control. The inhibition percentage was calculated using the following formula:

$$I\% = (C - T)/C \times 100$$

With C is the diameter of the positive control, while T is the diameter of inhibition of the sample.

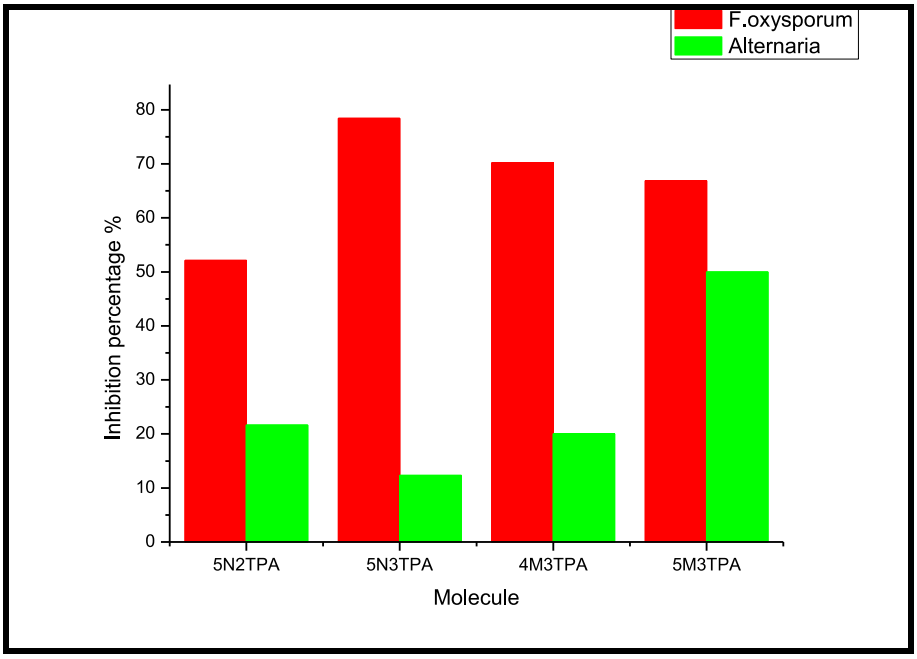

Fig. 4. The antifungal activity of the studied molecules expressed by inhibition percentage against two fungi: *Fusarium oxysporum* and *Alternaria alternata.*

Table 4
Diameter of the inhibition zone (mm) of the studied molecules against *Fusarium oxysporum* and *Alternaria alternata.*

Molecule	Diameter of the inhibition zone (mm)			
	Fusarium oxysporum		*Alternaria alternata*	
	50 µg/ml	100µg/ml	50 µg/ml	100 µg/ml
5N2TPA	29.5 mm	27.3 mm	24 mm	23.5 mm
5N3TPA	39 mm	12.3 mm	27 mm	26.3 mm
4M3TPA	42 mm	17 mm	26 mm	24 mm
5M3TPA	26.5 mm	18.9 mm	25 mm	15 mm
C^+ DMSO	57 mm		30 mm	
C^- PDA	59 mm		49 mm	

PDA: Potato Dextrose Agar

Table 5
Inhibition percentage (I %) of the studied molecules against *Fusarium oxysporum* and *Alternaria alternata* at 100µg/ml.

Inhibition percentage (I%) at 100 µg/ml		
Molecule	*Fusarium oxysporum*	*Alternaria alternata*
5N2TPA	52.11	21.66
5N3TPA	78.42	12.33
4M3TPA	70.18	20.00
5M3TPA	66.84	50.00

Table 6
Calculated quantum chemical parameters of 5N2TPA, 5N3TPA, 4M3TPA and 5M3TPA using DFT at B3LYP/6-31G (d, p).

Quantum parameters	5N2TPA	5N3TPA	4M3TPA	5M3TPA
E_{HOMO} (a.u)	- 0.23011	- 0.24486	- 0.22224	- 0.21315
E_{LUMO} (a.u)	- 0.08404	- 0.09176	- 0.02007	- 0.01956
ΔE_{gap} (a.u)	- 0.14570	- 0.15310	- 0.20217	- 0.19359
Electron affinity (A)	0.23011	0.09176	0.22224	0.21315
Ionization Potential (I)	0.08404	0.24486	0.02007	0.01956
Chemical Potential (μ)	- 0.15707	- 0.16831	- 0.12115	- 0.11635
Global Hardness (η)	0.07303	0.07655	0.10108	0.09679
Global Softness (s)	13.69206	13.06335	9.89266	10.33111
Electronegativity (χ)	0.15707	0.16831	0.12115	0.11635
Electrophilicity (ω)	0.16890	0.18503	0.07260	0.06993
Dipole Moment (Debye)	5.0828	5.7279	2.9558	0.8082

2.6. Quantum chemical calculations

All quantum chemical calculations of the synthesized molecules were performed with GAUSSIAN 09 software [42]. Whereas, Gauss View was used for results visualizations and analysis, based on the density functional theory (DFT) in gas phase, employing Beck's three parameter hybrid exchange with Lee-Yang-Parr correlation functional (B3LYP) [43] at 6-31G (d,p) basis sets [44]. Furthermore, the energy values of the highest occupied molecular orbital (E_{HOMO}), lowest unoccupied molecular orbital (E_{LUMO}), energy gap (ΔE_{GAP}), Electron Affinity (A), Ionization Energy (I), electronic chemical potential (µ), molecular hardness (η), molecular softness (s), electronegativity (χ), electrophilicity index (ω) and dipole moment are calculated and presented in Table 6.

2.7. Molecular docking study

Molecular docking calculations were carried out using iGM-DOCK program version 2.1 to predict the binding mode of the investigated α-aminophosphonic acids on the Mpro binding site and to specify the interactions between inhibitors and the target protein. The structure of Mpro was obtained from Protein Data Bank (PDB ID: 6LU7) [45] and with a grid box of 30×30×30 Å. Accelry's Discovery Studio Visualizer was employed to explore the docked poses and 2D/3D interaction plots [46]. The obtained best docked models visualization of 5N2TPA, 5N3TPA, 4M3TPA and 5M3TPA with SARS-CoV-2 main protease are presented in Fig. 7.

3. Results and discussion

3.1. Spectroscopic study

The obtained synthesis yields of the studied α-aminophosphonates under microwave irradiations are between 86.95 and 96.98 % in a very short time. Moreover, the 4M3TPA was obtained directly after mixing the three components (amine, aldehyde and phosphonic acid) without microwave (Table 1). The structures of the synthesized molecules were confirmed by their spectroscopic data.

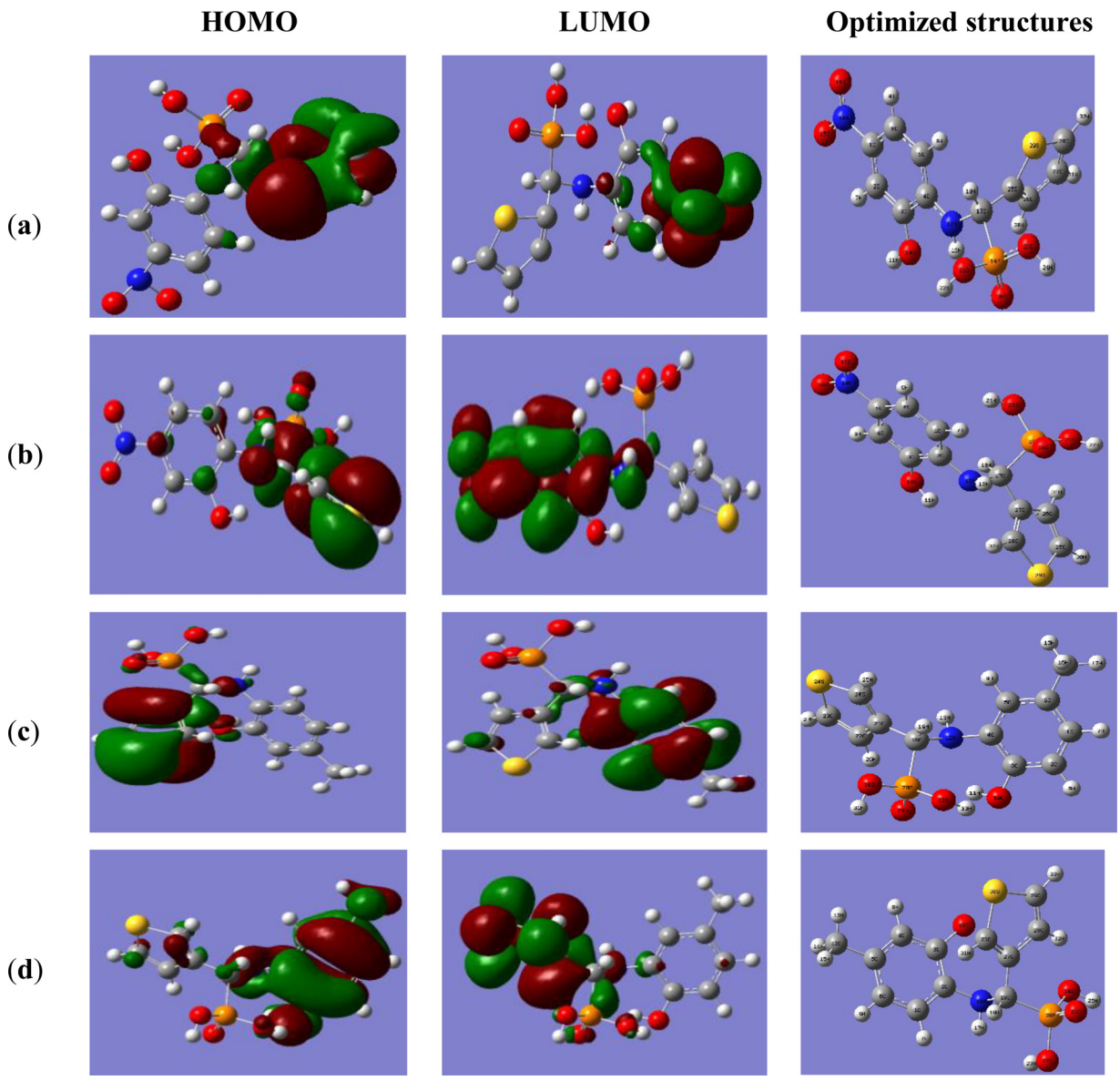

Fig. 5. 3D plots of frontier molecular orbitals (HOMO and LUMO) and the optimized structures of: (a) 5N2TPA, (b) 5N3TPA, (c) 4M3TPA and (d) 5M3TPA at the B3LYP/6-31G (d, p).

The experimental values of wavenumber and their assignments for the selected vibrations are summarized in Table 2. So, the examination of the results offered in Table 2 indicates the presence of the following vibrational modes: Firstly, the vibrational modes of the phosphonic acid group (-PO(OH)2), such as ν(P=O), ν(–OH), ν(P–O–H), and ν(C–P) are revealed as average to intense absorption peaks. So, peaks which are highest in wavenumber observed at 3597, 3594, 3577, and 3586 cm−1, respectively, are assigned to the stretching vibrations of O-H groups. Also, the detected peaks at 1252, 1276, 1262 and 1276 cm−1, respectively, are related to the stretching vibrations of the P=O groups. The situated peaks at 749, 742, 720 and 742 cm−1, respectively, may be attributed to the stretching modes of C–P groups. The clear peaks appeared at 930, 928, 945 and 943 cm−1, respectively, are associated to the deformation modes of (P-O-H) groups. Concerning the N-H groups, we can easily determine their stretching vibrations observing the presence of sharp peaks at higher wavenumbers. As a result, the symmetric and asymmetric stretching vibrations of N-H groups of 5N2TPA, 5N3TPA, 4M3TPA and 5M3TPA are situated at 3376, 3383, 3321 and 33375 cm−1, respectively. Regarding the C-H groups vibrations, we have the existence of both aromatic and aliphatic C-H stretching vibrations. Consequently, we can attribute the detected peaks between 3096, 3093, 3011 and 362 cm−1 to the asymmetric and symmetric stretching vibrations of the aromatic C-H groups. On the other hand, the observed peaks at 2916, 2902, 2901 and 2924 cm−1, respectively, may be attributed symmetric stretching modes of the aliphatic C-H groups, while the asymmetric stretching modes are observed at 2918, 2982, 2985 and 2886 cm−1, respectively. Moreover, the appeared peaks between 1400 and 1250 cm−1 are associated to the deformation modes of C-H functional groups. Usually, the characteristic peaks of stretching vibrations of the aromatic and aliphatic C-N groups of the studied compounds are located at 1015, 1002 cm−1, 1000 and 1002 cm−1, respectively. Finely, the stretching modes of the aromatic C-C groups are observed at 1400, 1399, 1453 and 1428 cm−1, respectively. The semicircular stretching vibrations of the aromatic C=C groups are located between 1610, 1606, 1605 and 1615 cm−1.

All the synthesized molecules exhibited infrared absorption bands for P=O, P-$C_{aliphatic}$ and C-N in the regions 1252-1276 cm^{-1}, 720-749 cm^{-1}, and 1000-1015 cm^{-1}, respectively. The peaks ap-

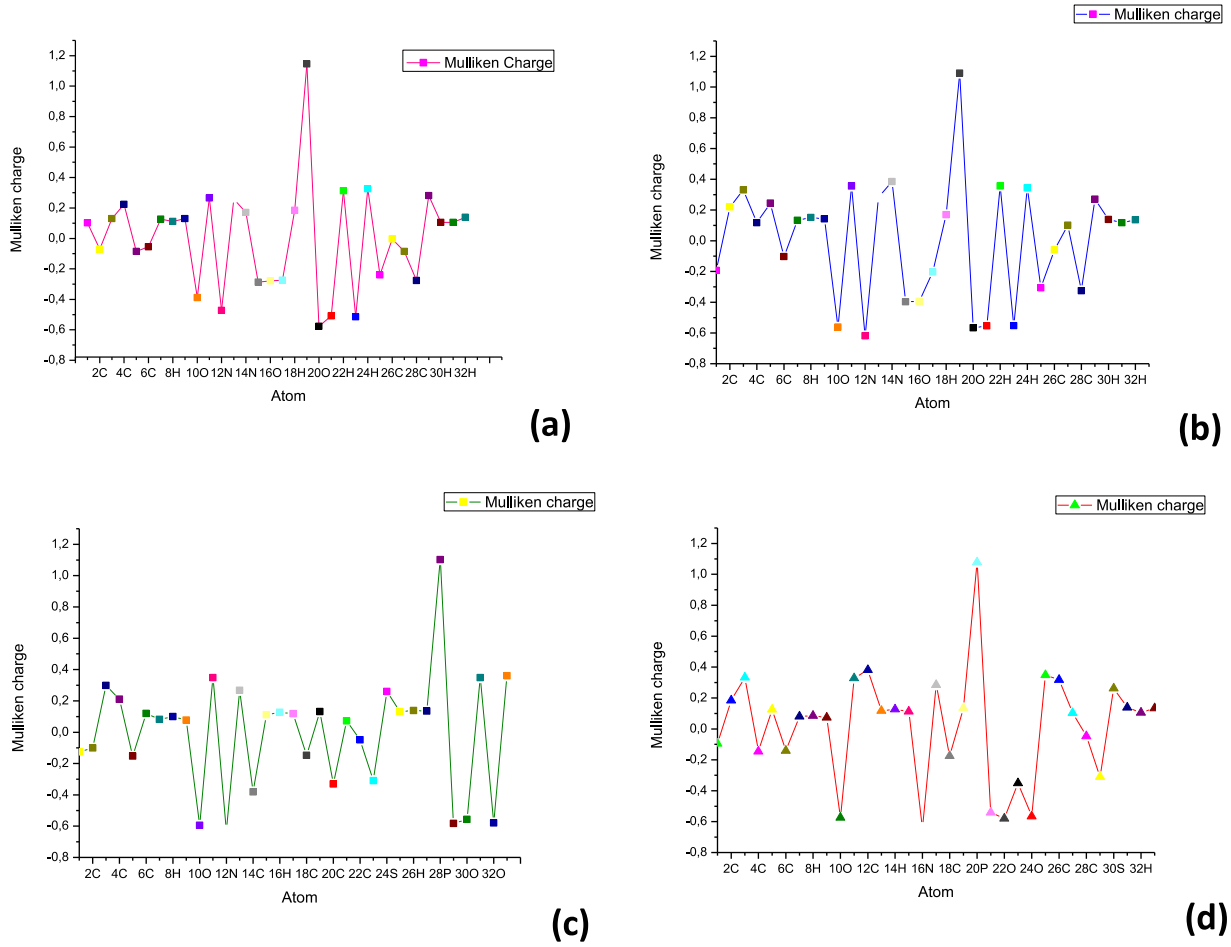

Fig. 6. Mulliken atomic charges of: (a) 5N2TPA, (b) 5N3TPA, (c) 4M3TPA and (d) 5M3TPA.

peared at 1605-1615 cm^{-1}, 1508-1516 cm^{-1}, 1064-1069 cm^{-1} and 928-945 cm^{-1} are correspond to the C=C, P-O-C and P-O-H functional groups, respectively. The appeared peaks at 2867-2904 cm^{-1} are attributed to the CH_3 functional group of 4M3TPA and 5M3TPA. The absence of the characteristic peaks of primary amine NH_2 and aldehyde (C=O), also the formation of new peaks may be confirms the formation of the proposed structures of α-aminophosphonic acids.

The UV-Vis spectra of the synthesized molecules (Fig. 2) show absorption bands in the ultraviolet region at 209-264 nm characteristic for a $\pi \rightarrow \pi^*$ transition, due to a conjugation in an unsaturated system. The bands appeared around 278-392 nm are attributed to the $n \rightarrow \pi^*$ transition related to a conjugation with a system containing a lone pair of electrons (presence of hetero atoms N, O, S and P) [47].

The obtained NMR results confirm the chemical structures of the synthesized molecules. In this context, the ^{1}H NMR spectra show the presence of the characteristic chemical shifts of phenolic and theophenic protons at 6.60-7.61 ppm. Also, the characteristic chemical shifts for protons of C- **H**, P-O- **H** and N- **H** groups are appeared at 1.23-2.3 ppm, 5.91-5.93 ppm and 9.50 ppm, respectively. The ^{13}C NMR spectral data of the synthesized α-aminophosphonic acids showed the characteristic chemical shifts of the aromatic carbons of phenol and thiophene rings. The presence of the phosphorus atoms in all molecules is confirmed by ^{31}P NMR spectra. So, all signals of the investigated molecules were appeared between 2.95 and 3.51 ppm.

3.2. Antioxidant activity

The antioxidant activity of 5N2TPA, 5N3TPA, 4M3TPA and 5M3TPA was determined by three methods. Accordingly, the synthesized molecules show good activity against DPPH, Phenentroline and ABTS at very low concentrations. The obtained results are expressed in graphs which represent the percentage of inhibition against the sample concentration (Fig. 3).

3.2.1. Free radical scavenging activity (DPPH)

The violet color of the DPPH solution has been changed to residual pale yellow color, indicating that the studied α-aminophosphonic acids can donate a hydrogen atom which raises their reduced forms. The DPPH results of the investigated molecules were expressed as IC_{50} and their values are given in Table 3. Usually, the low value of IC_{50} gives the highest activity. Consequently, we observe that the 5N3TPA showed stronger antioxidant activity than standard BHT and than the other molecules with an IC_{50} of 16.04±0.4 µg/ml. On the other hand, the antioxidant activity of the synthesized α-aminophosphonates increases in the following order: BHA<5N3TPA< BHT <4M3TPA< 5M3TPA <5N2TPA.

3.2.2. ABTS scavenging

The obtained results of the ABTS assay are summarized in Table 3. The examination of these results shows that the tested molecules have a higher antioxidant activity and better than the

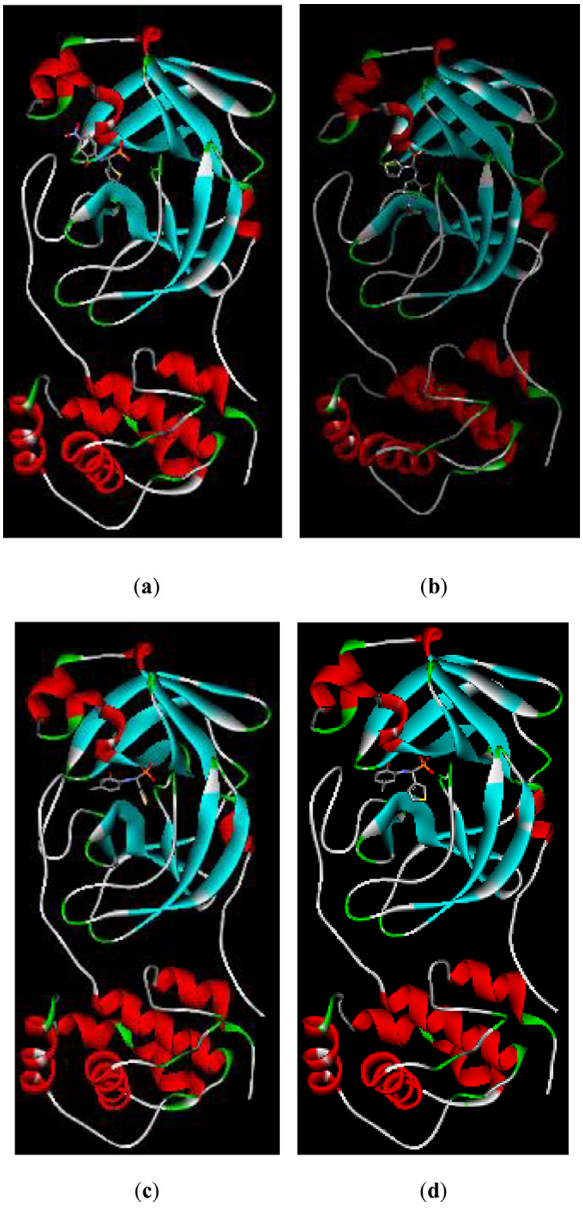

Fig. 7. Best docked models visualization of the investigated α-aminophosphonic acids with SARS-CoV-2 main protease: (a) 5N2TPA, (b) 5N3TPA, (c) 4M3TPA and (d) 5M3TPA.

BHA standard. Also, the antioxidant activity of the investigated compounds exhibits the following order: BHT<5N3TPA <4M3TPA< 5M3TPA < 5N2TPA < BHA.

3.2.3. Phenantroline

The obtained results of the phenantroline assay are expressed as $A_{0.5}$. Generally, the lowest value of $A_{0.5}$ gives the highest activity. Consequently, we observe from Table 3 that the 5N3TPA exhibits the highest activity and better than BHA with $A_{0.5} = 5.57 \pm 0.06$ µg/ml. on the other hand, the activity of the investigated α-aminophosphonic acids increases in the following order: BHT<5N3TPA<BHA<4M3TPA< 5M3TPA<5N2TPA (Table 3).

In general, the studied α-aminophosphonic acids showed a good antioxidant activity comparable to that of BHA and BHT standards. The presence of the aromatic ring, the thiophene ring and donor atoms (O, P, N and S) in the molecular structures of the studied molecules enhances their bioactivity. The high activity of 5N3TPA may be due to the presence of the nitro group on the *orto* position of the phenol ring and attached with the 3-thiophene, compared with 5N2TPA which contains the same substitution but it attached with the 2-thiophene. Also, it shows a better activity than the molecules substituted with methyl group (4M3TPA and 5M3TPA). On the other hand, the 4M3TPA substituted with a methyl group at the *para* position is more reactive than 5M3TPA substituted by the same group at the *orto* position.

Table 7
Molecular docking results and interactions of the investigated inhibitors with SARS-CoV-2 main protease.

Compounds	Binding energy in kcal/mol	Interactions
5N2TPA	- 106.1	Elc: HIS41 H-bonds: HIS41, TYR54, CYS145, HIS164 vdW: HIS41, MET49, HIS164, MET165, GLN189
5N3TPA	- 105.2	H-bonds: HIS41, GLY143, SER144, CYS145, HIS163, GLU166 vdW: HIS41, LEU141, ASN142, GLY143, CYS145, HIS163, HIS164
4M3TPA	- 102.9	H-bonds: HIS41, GLY143, SER144, CYS145, HIS164 vdW: LEU141, ASN142, MET165, GLU166, GLN189
5M3TPA	- 101.9	H-bonds: HIS41, GLY143, SER144, CYS145, HIS164 vdW: LEU141, ASN142, MET165, GLU166, GLN189

Elc: electrostatic interactions, H-bonds: hydrogen bonding and vdW: van der Waals forces

3.3. Antifungal activity

The antifungal activity of the synthesized molecules was tested against two fungi, *Fusarium oxysporum* and *Alternaria alternata* by the disc diffusion method. The obtained results were expressed by the diameter of the inhibition zone (Table 4) and the inhibition percentage (Table 5). The growth of both fungi was clearly inhibited by the studied α-aminophosphonic acids. Moreover, *Fusarium oxysporum* was better inhibited than *Alternaria alternata*. The antifungal activity increased with increasing the concentration and the 5N3TPA exhibits the best inhibition capacity (I% = 78.42 % at 100 µg/ml). The presence of active functionalities on the aromatic ring, P=O and P-OH groups of α-aminophosphonates and thiophene motif enhances the antifungal activity of the studied compounds (Fig. 4).

3.4. Computational study

3.4.1. Optimized structures

The optimized structures and the numbering of atoms of 5N2TPA, 5N3TPA, 4M3TPA and 5M3TPA obtained at B3LYP/6-31G (d,p) are shown in Fig. 5.

3.4.2. Frontier molecular orbitals (FMOs)

Frontier molecular orbitals (FMOs) play an important role in determining the electronic properties and the chemical reactivity of molecules [48, 49]. LUMO (lowest unoccupied molecular orbital) is able to accept an electron, while HOMO (highest occupied molecular orbital) is able to donate an electron. The calculated isodensities of HOMO and LUMO of the investigated molecules are presented in Fig. 5. We can notice two colors green and red; the green color represents the negative phase while the red color corresponds to the positive phase. The electron density of HOMO is concentrated on the thiophene ring for 5N2TPA, 5N3TPA and 5M3TPA but it

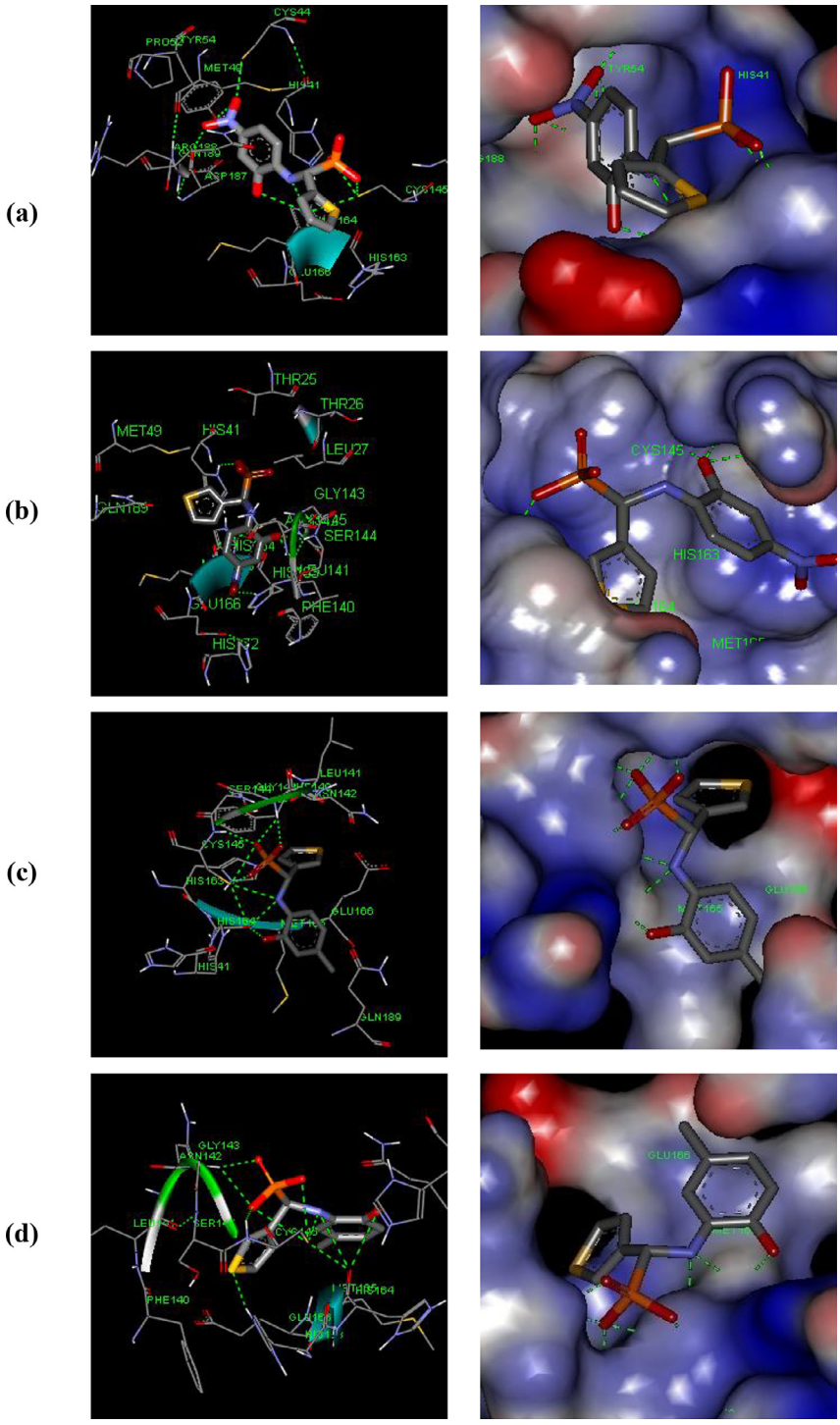

Fig. 8. Left: 3D Binding-interaction diagrams of the studied inhibitors with SARS-CoV-2 main protease (a) 5N2TPA, (b) 5N3TPA, (c) 4M3TPA and (d) 5M3TPA. Right: Inside binding sites.

Table 8
Energy distribution of the investigated inhibitors between van der Waals forces, hydrogen bonding and electrostatic interactions.

Ligand	van der Waals forces	hydrogen bonding	electrostatic interactions
5N2TPA	- 72.9863	- 28.8757	- 3.22359
5N3TPA	- 78.048	- 25.7353	- 1.37457
4M3TPA	- 67.7466	- 33.0763	- 1.12479
5M3TPA	- 68.9712	- 32.7829	- 1.11344

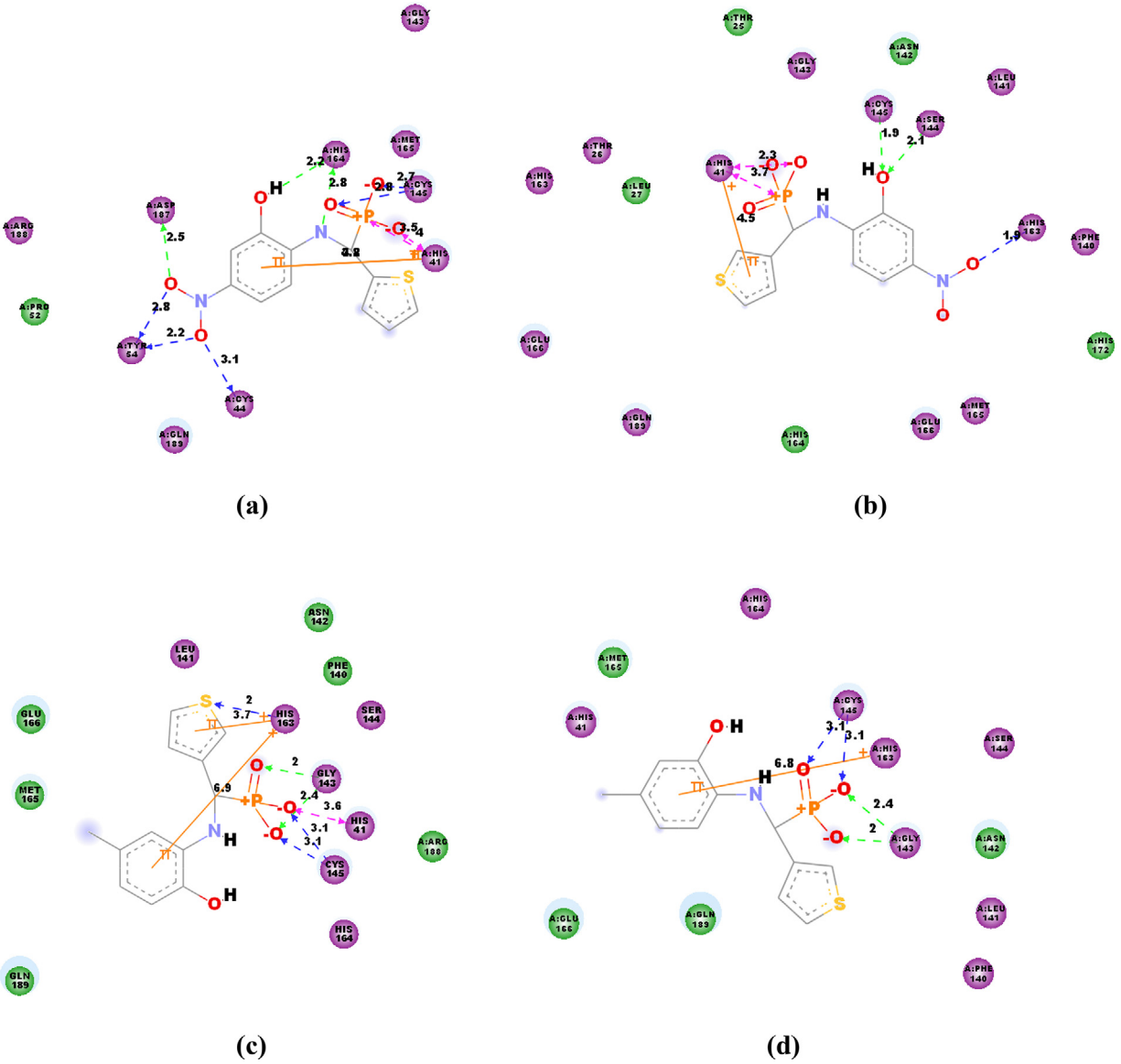

Fig. 9. 2D Binding-interaction diagrams of the studied inhibitors with SARS-CoV-2 main protease (a) 5N2TPA, (b) 5N3TPA, (c) 4M3TPA and (d) 5M3TPA.

is concentrated on aminophenol ring (aromatic ring) for 4M3TPA. Also, the isodensity of LUMO is localized on the aromatic ring for 5N2TPA, 5N3TPA and 5M3TPA, whereas it is focused on the thiophene ring for 4M3TPA. From Table 6, we observe that the HOMO-LUMO gap energy (ΔE_{GAP}) increases in the order $\Delta E_{GAP\ (4M3TPA)} < \Delta E_{GAP\ (5M3TPA)} < \Delta E_{GAP\ (5N3TPA)} < \Delta E_{GAP\ (5N2TPA)}$, this means that 4M3TPA and 5M3TPA exhibit easy the electrons flow. Moreover, the chemical potential index of 5M3TPA (μ = - 0.11) and 4M3TPA (μ = - 0.12) are greater than these of the other molecules, which means that these two molecules behaves as good donors of electrons. Furthermore, the electronegativity and the dipole moment of 5N3TPA are higher than the other studied molecules ($\chi = 0.168$ and $D = 5.737$), which makes this molecule more reactive and able to attract electrons. The electrophilicity index increases in the order: $\omega_{(5M3TPA)} < \omega_{(4M3TPA)} < \omega_{(5N2TPA)} < \omega_{(5N3TPA)}$, which means that the accepting ability of electrons is higher for 5N3TPA.

3.4.3. Mulliken atomic charges

The calculated values of Mulliken atomic charges for the studied molecules are presented in Fig. 6. The C1/C3/C4, C2/C3/C5/C27, C3/C4/C6/C21 and C2/C3/C5/C27 atoms of 5N2TPA, 5N3TPA, 4M3TPA and 5M3TPA, respectively, exhibit positive charges while the other carbon atoms have negative charges. In all molecules, the phosphorus atoms have a maximum positive charge values between (1.145, 1.098, 1.102 and 1,078), respectively, while the oxygen atoms of phosphonic groups have maximum negative charges (-0.577 and -0.565) for 5N2TPA and 5N3TPA (substituted with nitro group). On the other hand, the nitrogen atoms of 4M3TPA and 5M3TPA (substituted with methyl group) have the maximum negative charges (-0.625 and -0.639). Moreover, the hydrogen and sulfur atoms have positive charges. The negative charges on oxygen atoms indicate the ability to form H-bonds. Furthermore, the positively charged centers are the most susceptible sites for nucleophilic attack, while the negative sites are susceptible for electrophilic one [50].

3.5. Molecular docking study

The binding energy and the interaction types of the investigated α-aminophosphonic acids with Mpro are presented in Table 7. So, the calculated values of the binding energy of the studied ligands indicate that 5N2TPA inhibits Mpro more than 5N3TPA, 4M3TPA and 5M3TPA.

From the 2D plots presented in Fig. 9, we can notice that 5N2TPA interacts with amino acid residues in the active site through H-bonds with HIS41 at a distance of 3.54 Å, TYR54 (2.2 and 2.8 Å), CYS145 (2.7 and 2.8 Å), HIS164 (2.8 and 2.2 Å), a Pi-sulfur interaction between the phenol ring of the ligand and HIS41 at a distance of 4.2 Å, electrostatic bond with HIS41 and Van der Waals bonds with HIS41, MET49, HIS164, MET165, and GLN189. The obtained value of the binding energy of 5N2TPA is - 106.1 kcal/mol. Moreover, the 5N3TPA ligand forms H-bonds with HIS41 (2.3 and 3.7 Å), GLY143, SER144 (2.1 Å), CYS145 (1.9 Å), HIS163 (1.9 Å) and GLU166, and forms a Pi-sulfur interaction between the thiophene ring of the ligand and HIS41 at a distance of 4.5 Å. Also, vdW forces are present with HIS41, LEU141, ASN142, GLY143, CYS145, HIS163 and HIS164. The calculated value of the binding energy for 5N3TPA is - 105.2 kcal/mol. In addition, the 4M3TPA interacts with the target protein with a binding energy equal to - 102.9 kcal/mol. Accordingly, 4M3TPA forms hydrogen bonds with HIS41 (3.6 Å), GLY143 (2 and 2.4 Å), SER144, CYS145 (3.1 and 3.1 Å) and HIS164 and forms two Pi-sulfur interactions between HIS163 and thiophene ring at a distance of 3.7 Å, and with the aromatic ring (phenol) at a distance of 6.9 Å. Also, vdW interactions are formed between 4M3TPA and LEU141, ASN142, MET165, GLU166 and GLN189 amino acid residues of Mpro. On the other hand, the 5M3TPA ligand forms H-bonds with HIS41 (2 Å), GLY143 (2.4 Å), SER144 (3.1 Å), CYS145 (3.1 Å) and HIS164, and a Pi-sulfur interaction between the phenol ring of the ligand and HIS163 at a distance of 6.8 Å. Furthermore, vdW forces have been observed with LEU141, ASN142, MET165, GLU166 and GLN189. Concerning 4M3TPA ligand, the calculated value of the binding energy is - 101.9 kcal/mol. As a result, the obtained docking results show that 5N2TPA, 5N3TPA, 4M3TPA and 5M3TPA penetrate well into the active areas of the protein. Therefore, these molecules can be considered to be potent inhibitors against COVID-19 disease.

The energy distribution of the investigated inhibitors between van der Waals forces, hydrogen bonding and electrostatic interactions are presented in Table 8. The docking calculations led to the following results: the 4M3TPA ligand possesses the strongest van der Waals interactions (E_{vdW} = - 67.7466 kcal/mol), while the 5N3TPA showed the highest hydrogen bonding energy ($E_{H\text{-}bond}$ = - 25.7353 kcal/mol). Also, the electrostatic interactions were found to be higher for 5M3TPA ($E_{(5M3TPA)}$ = - 1.11344 kcal/mol).

4. Conclusion

In the present paper, four α-aminophosphonic acids 5N2TPA, 5N3TPA, 4M3TPA and 5M3TPA were synthesized and evaluated for their biological activities. The antioxidant activities determined by the DPPH method, ATBS scavenging and phenantroline assay indicated that all compounds could be considered as potential antioxidants at very low concentrations and being more active than BHT and BHA standards. The investigated compounds exhibited a potent anti-fungal activity. The experimental results revealed that the 5N3TPA exhibits the best activity (antioxidant and anti-fungal), which is confirmed by the theoretical study (DFT). The high activity of 5N3TPA may be due to the presence of the nitro group and the heterocyclic ring. Furthermore, the molecular docking investigation shows that the studied molecules could be considered as potential inhibitors against SARS-CoV-2 main protease responsible of Coronavirus disease.(Fig. 8)

Declaration of Competing Interest

The authors declare that they have no known competing financial interests or personal relationships that could have appeared to influence the work reported in this paper.

CRediT authorship contribution statement

Hamida Tlidjane: Writing – original draft, Writing – review & editing, Project administration, Data curation, Formal analysis, Resources, Investigation. **Nadjib Chafai:** Conceptualization, Methodology, Validation, Writing – original draft, Supervision, Project administration, Resources, Investigation. **Salah Chafaa:** Project administration, Supervision, Writing – review & editing, Funding acquisition. **Chawki Bensouici:** Supervision, Resources. **Khalissa Benbouguerra:** Supervision, Writing – review & editing.

Acknowledgments

The authors greatly acknowledge the General Directorate for Scientific Research and Technological Development (DGRSDT), Algerian Ministry of Scientific Research, Laboratory of Electrochemical of Molecular Materials and Complex (LEMMC), Ferhat ABBAS University of Setif-1, Algeria. Also, authors thank the Biotechnologie Research Center CRBt.

References

[1] N. Zhu, D. Zhang, W. Wang, X. Li, B. Yang, J. Song, X. Zhao, B. Huang, W. Shi, R. Lu, P. Niu, F. Zhan, X. Ma, D. Wang, W. Xu, G. Wu, G.F. Gao, W. Tan, A novel corona virus from patients with pneumonia in China, N. Engl J .Med. 382 (2020) 727–733.
[2] C. Huang, Y. Wang, X. Li, L. Ren, J. Zhao, Y. Hu, L. Zhang, G. Fan, J. Xu, X. Gu, Z. Cheng, T. Yu, J. Xia, Y. Wei, W. Wu, X. Xie, W. Yin, H. Li, M. Liu, Y. Xiao, H. Gao, L. Guo, J. Xie, G. Wang, R. Jiang, Z. Gao, Q. Jin, J. Wang, B. Cao, Clinical features of patients infected with 2019 novel coronavirus in Wuhan, China, Lancet 395 (2020) 497–506.
[3] WHO, WHO Corona virus Disease (COVID-19) Dashboard. Gneva, World Health Organization (2020).
[4] H. Lu, C.W. Stratton, Y. Tang, Outbreak of pneumonia of unknown etiology in Wuhan, China: The mystery and the miracle, Med. Virol. 92 (2020) 401–402.
[5] S.C. Fields, Synthesis of natural products containing a C-P bond, Tetrahedron 55 (1999) 12237.
[6] J. Liu, S. Yang, X. Li, H. Fun, P. Bhadury, W. Xu, J. Wu, Z. Wang, Synthesis and antiviral bioactivity of chiral thioureas containing leucine and phosphonate moieties, Molecules 15 (2010) 5112–5123.
[7] J. Huang, R. Chen, An overview of recent advances on the synthesis and biological activity of α-aminophosphonic acid derivatives, Heteroatom Chem. 11 (2000) 480–492.
[8] K.M.K. Reddy, S.M. Sadik, N. Saichaithanya, K. Peddana, N.B. Reddy, G. Sravya, G.V Zyryanov, C.S. Reddy, One-pot green synthesis and cytotoxicity of new α-aminophosphonates, Res. Chem. Intermed. 43 (2017) 7087–7103.
[9] C.B. Reddy, K.S. Kumar, M.A. Kumar, M.V.N. Reddy, B.S. Krishna, M. Naveen, M.K. Arunasree, C.S. Reddy, C.N. Raju, C.D. Reddy, PEG-SO_3H catalyzed synthesis and cytotoxicity of α-aminophosphonates, Eur. J. Med. Chem. 47 (2012) 553–559.
[10] A.A.S. Ahmed, H.M. Awad, I.E.T. El-Sayed, A.A. El Gokha, Synthesis and antiproliferative activity of new hybrids bearing neocryptolepine, acridine and α-aminophosphonates scaffolds, J. Iran. Chem. Soc. 17 (2020) 1211–1221.
[11] S. De Lombaert, L. Blanchard, J. Tan, Y. Sakane, C. Berry, R.D. Ghai, Non-peptidic inhibitors of neutral endopeptidase 24.11 1. Discovery and optimization of potency, Bioorg. Med. Chem. Lett. 5 (1995) 145–150.
[12] M.C. Allen, W. Fuhrer, B. Tuck, R. Wade, J.M. Wood, Synthesis of transition-state analog inhibitors containing phosphorus acid derivatives at the scissile bond, J. Med. Chem. 32 (1989) 1652–1661.
[13] P. Kafarski, B. Lejczak, Biological activity of aminophosphonic acids, Phosphorus Sulfur Silicon Rel. 63 (1991)193-215.
[14] R. Damiche, S. Chafaa, Synthesis of new bioactive aminophosphonates and study of their antioxidant, anti-inflammatory and antibacterial activities as well the assessment of their toxicological activity, J. Mol. Struct. 1130 (2017) 1009–1017.
[15] J. Lewkowski, Z. Malinowski, A. Matusiak, M. Morawska, D. Rogacz, P. Rychter, The Effect of New Thiophene-Derived Aminophosphonic Derivatives on Growth of Terrestrial Plants: a Seedling Emergence and Growth Test, Molecules 21 (2016) 694.
[16] D. Rogacz, J. Lewkowski, Z. Malinowski, A. Matusiak, M. Morawska, P. Rychter, Effect of New Thiophene-Derived Aminophosphonic Derivatives on Growth of Terrestrial Plants. Part 2. Their Ecotoxicological Impact and Phytotoxicity Test Toward Herbicidal Application in Agriculture, Molecules 23 (2018) 3173.
[17] Z.Frouzabadi Rezaei, H. Irarpoor, N. Ghaderi, A. Jafari, M.R. Zare, HR, Design and one pot synthesis of α-aminophosphonates and bis (α-aminophosphonates) by iron(III) and cytotoxic activity, Eur. J. Med. Chem. 44 (2009) 4266–4275.
[18] N. Chafai, S. Chafaa, K. Benbouguerra, D. Daoud, A. Hellal, M. Mehri, Synthesis, characterization and the inhibition activity of a new α-aminophosphonic

derivative on the corrosion of XC48 carbon steel in 0.5 M H_2SO_4: Experimental and theoretical studies, J. Taiwan Inst. Chem. Eng. 70 (2017) 331–344.
[19] M. Djenane, S. Chafaa, N. Chafai, R. Kerkour, A. Hellal, Synthesis, spectral properties and corrosion inhibition efficiency of new ethylhydrogen[(methoxyphenyl)(ethyl amino)methyl]phosphonate derivatives: Experimental and theoretical investigation, J. Mol. Struct. 1175 (2018) 398–413.
[20] O. Moumeni, S. Chafaa, R. Kerkour, K. Benbouguerra, N. Chafai, Synthesis, structural and anticorrosion properties of diethyl(phenylamino)methyl) phosphonate derivatives: experimental and theoretical study, J. Mol. Struct. 1206 (2020) 127693.
[21] S. Chandrasekhar, S.J. Prakash, V. Jagadeshwar, Ch. Narsihmulu, Three components coupling catalyzed by $TaCl_5$-SiO_2: synthesis of aminophosphonates, Tetrahedron. Lett. 42 (2001) 5561.
[22] B.C. Ranu, A. Hajra, U. Jana, General Procedure for the Synthesis of α-aminophosphonate from Aldehydes and Ketones Using Indium (III) Chloride as a Catalyst, Org. Lett. 1 (1999) 1141.
[23] M. Hosseini- Sarvari, TiO_2 as a new and reusable catalyst for one-pot three--component syntheses of α-aminophosphonates in solvent-free conditions, Tetrahedron 64 (2008) 5459–5466.
[24] L. Macarie, V. Simulescu, G. Ilia, Ultrasonic irradiation used in synthesis of aminophosphonates, Monatsh Chem. 150 (2019) 163–171.
[25] M.H. Basha, C. Subramanyam, K.P. Rao, Ultrasound-promoted solvent-free synthesis of some new α-aminophosphonates as potential antioxidants, Main Group Metal Chem. 43 (2020) 147–153.
[26] E.L. Loredo-Calderón, C.A. Velázquez-Martínez, M.A. Ramírez-Cabrera, E. Hernández-Fernández, V.M. Rivas-Galindo, E.A. Espinoza, S.T. López-Cortina, Synthesis of novel α-aminophosphonates under microwave irradiation, biological evaluation as antiproliferative agents and apoptosis inducers, Med. Chem. Res. 28 (2019) 2067–2078.
[27] Á. Tajti, E. Bálint, G. Keglevich, Microwave-assisted synthesis of α-aminophosphonates and related derivatives by the Kabachnik-Fields reaction, Phosphorus, Sulfur, Silicon Relat. Elem. (2019) 379–381.
[28] A. Hellal, S. Chafaa, N. Chafai, Synthesis, characterization and computational studies of three α-amino-phosphonic acids derivatives from Meta, Ortho and Para aminophenol, J. Mol. Struct. 1103 (2016) 110–124.
[29] M. Mehri, N. Chafai, L. Ouksel, K. Benbouguerra, A. Hellal, S. Chafaa, Synthesis, electrochemical and classical evaluation of the antioxidant activity of three α-aminophosphonic acids: Experimental and theoretical investigation, J. Mol. Struct. 1171 (2018) 179–189.
[30] N. Chafai, S. Chafaa, K. Benbouguerra, A. Hellal, M. Mehri, Synthesis, spectral analysis, anti-corrosive activity and theoretical study of an aromatic hydrazone derivative, J. Mol. Struct. 1181 (2019) 83–92.
[31] X.J. Mu, M.Y. Lei, J.P. Zou, W.Wei W. Zhang, Microwave-assisted solvent-free and catalyst-free Kabachnick-Fields reactions for α-aminophosphonates, Tetrahedron. Lett. 47 (7) (2006) 1125–1127.
[32] G. Keglevich, A. Szekrenyi, Eco-friendly accomplichment of the extended Kabachnick-Fields reaction: a solvent and catalyst-free microwave assisted synthesis of α- aminophosphonates and α-aminophosphine oxides, Lett. Org. Chem. 5 (2008) 616–622.
[33] E. Balint, A. Tajti, D. Kalocsai, B. Matravolgyi, K. Karaghiosoff, M. Czugler, G. Keglevich, Synthesis and utilization of optically active aminophosphonates derivatives by Kabachnick-Fields reaction, Tetrahedron 73 (2017) 5659–5667.
[34] S. Zaout, S. Chafaa, A Hellal, O. Boukhemis, L. Khattabi, H. Merazig, N. Chafai, C. Bensouici L. Bendjeddou, Hydroxyphenylamine phosphonate derivatives: synthesis, X-ray crystallographic analysis, and evaluation of theirs anti-Alzheimer effects and antioxidant activities, J. Mol. Struct. 1225 (2021) 129121.
[35] N. Houas, S. Chafaa, N. Chafai, S. Ghedjati, M. Djenane, S. Kitouni, Synthesis, characterization, DFT study and antioxidant activity of (2-hydroxynaphthalen-1-yl) methyl 2-hydroxyphenyl amino phosphonic acid, J. Mol. Struct. 1247 (2021) 131322.
[36] K. Benbouguerra, S. Chafaa, N. Chafai, M. Mehri, O. Moumeni, A. Hellal, Synthesis, spectroscopic characterization and a comparative study of the corrosion inhibitive efficiency of an α-aminophosphonate and Schiff base derivatives: experimental and theoretical investigations, J. Mol. Struct. 1157 (2018) 165–176.
[37] K. Benbouguerra, N. Chafai, S. Chafaa, Y.I. Touahria, H. Tlidjane, New α-Hydrazinophosphonic acid: synthesis, characterization, DFT study and *in silico* prediction of its potential inhibition of SARS-CoV-2 main protease, J. Mol. Struct. 1239 (2021) 130480.
[38] M.S. Blois, Antioxidant determinations by the use of a stable free radical, Nature 4617 (181) (1958) 1119–1200.
[39] R. Re, N. Pellegrini, A. Proteggente, A. Pannala, M. Yang, C. Rice-Evans, Antioxidant activity applying an improved ABTS radical cation decolorization assay, Free Radical Bio. Med. 26 (1999) 1231–1237.
[40] A. Szydlowska-Czerniaka, C. Dianoczki, K. Recseg, G. Karlovits, E. Szlyk, Determination of antioxidant capacities of vegetable oils by ferric-ion spectrophotometric methods, Talanta 76 (2008) 899–905.
[41] A.W. Bauer, M.M. Kirby, J.C. Sherris, M. Truck, Antibiotic susceptibility testing by a standardized single disk method, Am. J. Clin. Pathol. 45 (1966) 493–496.
[42] M.J. Frisch, G.W. Trucks, H.B. Schlegel, G.E. Scuseria, M.A. Robb, J.R. Cheeseman, G. Scalmani, V. Barone, B. Mennucci, G.A. Petersson, H. Nakatsuji, M. Caricato, X. Li, H.P. Hratchian, A.F. Izmaylov, J. Bloino, G. Zheng, J.L. Sonnenberg, M. Hada, M. Ehara, K. Toyota, R. Fukuda, J. Hasegawa, M. Ishida, T. Nakajima, Y. Honda, O. Kitao, H. Nakai, T. Vreven, J.A. Montgomery Jr., J.E. Peralta, F. Ogliaro, M. Bearpark, J.J. Heyd, E. Brothers, K.N. Kudin, V.N. Staroverov, R. Kobayashi, J. Normand, K. Raghavachari, A. Rendell, J.C. Burant, S.S. Iyengar, J. Tomasi, M. Cossi, N. Rega, J.M. Millam, M. Klene, J.E. Knox, J.B. Cross, V. Bakken, C. Adamo, J. Jaramillo, R. Gomperts, R.E. Stratmann, O. Yazyev, A.J. Austin, R. Cammi, C. Pomelli, J.W. Ochterski, R.L. Martin, K. Morokuma, V.G. Zakrzewski, G.A. Voth, P. Salvador, J.J. Dannenberg, S. Dapprich, A.D. Daniels, O. Farkas, J.B. Foresman, J.V. Ortiz, J. Cioslowski, D.J. Fox, Gaussian 09, Revision A.02, Gaussian, Inc., Wallingford, CT, 2009.
[43] C. Lee, W. Yang, R.G Parr, Development of the Colle-Salvetti correlation-energy formula into a functional of the electron density, Phys. Rev B. 37 (1998) 785–789.
[44] A.D. Beck, Density-functional thermochemistry. III. The role of exact exchange, J. Chem. Phys. 98 (1993) 5648–5652.
[45] C.D. Owen, P. Lukacik, C.M. Strain-Damerell, A. Douangamath, A.J. Powell, D. Fearon, J. Brandao-Neto, A.D. Crawshaw, D. Aragao, M. Williams, R. Flaig, D.R. Hall, K.E. McAuley, M. Mazzorana, D.I. Stuart, F. von Delft, M.A. Walsh, SARS-CoV-2 main protease with unliganded active site (2019-nCoV, coronavirus disease 2019, COVID-19). RCSB Protein Data Bank (PDB) ID, 6Y84, 3-7.https://doi.org/10.221/pdb6Y84.
[46] Biovia D.S. Discovery studio visualizer, Dassault System. (2019) (v19.1.0.15350).
[47] R. Anderson, D. Bendell, P. Groundwater, in: Organic Spectroscopic Analysis, 22, Royal Society of Chemistry, Cambridge, United Kingdom, 2004, pp. 7–23.
[48] A.M. Asiri, M. Karabacack, M. Kurt, K.A. Alamry, Synthesis, molecular conformation, vibrational and electronic transition, isometric chemical shift, polarizability and hyperpolarizability analysis of 3-(4-Methoxy-phenyl)-2-(4-nitro-phenyl)-acrylonitrile: a combined experimental and theoretical analysis, Spectrochim. Acta. A. 82 (2011) 444–455.
[49] B. Kosar, C. Albayrak, Spectroscopic investigations and quantum chemical computational study of (*E*)-4-methoxy-2-[(p-tolylimino)methyl]phenol, Spectrochim. Acta. A. 78 (2011) 160–167.
[50] T.A. Yousef, Stuctural, optical morphology characterization and DFT studies of nano sized Cu (II) complexes containing Schiff base using green synthesis, J. Mol. Struc. 1215 (2020) 128–180.